ORIGINAL RESEARCH

Promotion of skin regeneration through co-axial electrospun fibers loaded with basic fibroblast growth factor

Jialong Chen[1,2] · Guo Zhang[1,2] · Yang Zhao[1,2] · Muran Zhou[1,2] · Aimei Zhong[1,2] · Jiaming Sun[1,2]

Abstract

Cutaneous wound healing is complex, requiring a coordinated response by growth factors, drugs, and resident cells of the skin. To simulate native extracellular matrix, electrospun nanofibers offer a favorable microenvironment for biological processes, generating considerable interest in skin tissue regeneration. Furthermore, among the most essential growth factors in wound healing, basic fibroblast growth factor (bFGF) promotes cell migration, proliferation, and differentiation, thus enhancing wound healing. However, its application is limited by a short half-life and loss of bioactivity in normal physiological conditions when used in its naked form and without stabilization. Hence, delivering the growth factor with a controllable releasing speed constitutes a challenge. The aim of this study was to create a growth factor-releasing system that allows for time-controlled release to facilitate skin regeneration. Electrospun collagen-graphene oxide (Col-GO) scaffolds loaded with bFGF were fabricated. The cumulative release rate of the Col-0.2% GO-bFGF group was $30.94 \pm 7.77\%$, which was superior to the other groups. Moreover, core–shell structured Col/GO and polylactic acid (PLA) nanofibers were fabricated by coaxial electrospinning in the attempt of reducing the degradation rate of the scaffolds (Col-GO). The ability of the materials to promoting wound healing in vitro and in vivo was investigated, and the improved skin tissue recovery with the growth factor release system was demonstrated. Importantly, bFGF was sustained-released through the constructed systems, leading to the best wound healing performance when the scaffolds contained the growth factor. The healing rates of Col-GO and core–shell scaffolds loaded with bFGF were $96.39 \pm 0.66\%$ and $92.29 \pm 0.42\%$, respectively.

Keywords Graphene oxide · Collagen · Sustained release · Basic fibroblast growth factor (bFGF) · Wound healing · Co-axial electrospinning

1 Introduction

Skin injuries resulting from surgery, trauma, diabetes, or other chronic wounds are among the most common ailments in the clinic [1, 2]. Globally, they represent one of the most challenging healthcare burdens, both economically and socially, considerably affecting the life quality of patients [3–5]. In fact, the wound care market is predicted to continue growing in the next years, due to the constant increase of the elderly population and because of the detrimental impact of modern lifestyles all around the world [4]. Hence, new solutions are crucial to improve and more effectively promote wound healing.

It is known that wound healing is a dynamic and complex process involving inflammation, proliferation, and remodeling [6]. However, the aim of traditional wound care is merely to support healing by stopping bleeding and preventing infection. In this prospect, temporary biomaterials with proven biocompatibility are utilized only as physical barriers, with little consideration of their effect on the biological aspect of the wound healing process. Hence, over the past decades, research efforts have led to the development of bioactive wound dressings with the ability to promote and instruct healing at the molecular level, building from

---

Jialong Chen and Guo Zhang contributed equally to this work.

✉ Aimei Zhong
aimei_zhong@hust.edu.cn

✉ Jiaming Sun
sunjm1592@sina.com

1 Department of Plastic Surgery, Union Hospital, Tongji Medical College, Huazhong University of Science and Technology, Wuhan 430022, China

2 Wuhan Clinical Research Center for Superficial Organ Reconstruction, Wuhan 430022, China

both natural and synthetic biomaterials such as collagen [7], chitosan [8], silk proteins [9], cellulose [10], and polyurethane among others [11]. However, most of those fail to be cost-effective and/or are not readily applicable in the clinic, inciting for improved and readily available wound dressings. Currently, the technology of electrospinning offers a simple, controllable, and scalable process for the fabrication of fibrous scaffolds which constitute one of the best candidate dressings, due to their fibrous nature mimicking the natural extracellular matrix (ECM) of skin tissue [12]. Moreover, by design, electrospinning can reproduce the topography of skin tissue [13], which has shown substantial regulatory effects on cellular behavior [14, 15]. Other important advantages include the ability of electrospun materials to retain moisture [16] and serve as a drug carrier [17] with releasing properties. In addition, electrospinning technology is rapidly evolving from a single fluid solution blending electrospinning [18] to coaxial [19] and modified coaxial electrospinning [20], which expands its ability to encapsulate active ingredients [21]. Particularly, coaxial electrospinning has broadly demonstrated to be useful for manipulating the drug release profiles of fast [22], and multiple-phase release used on the core–shell polymer-based nanohybrids and can act as a strong platform for developing biphasic release dosage forms. Here are new interesting applications of this nanostructure.

Besides the choice of the biomaterial, the use of bioactive small molecules such as growth factors plays an important role in enhancing wound healing. At the molecular level, they interact with cells and guide their behavior. Several growth factors have been identified to improve healing, such as the basic fibroblast growth factor (bFGF), fibroblast growth factor-2 (FGF2), vascular endothelial growth factor (VEGF), epidermal growth factor (EGF), and platelet-derived growth factor (PDGF), which can enhance cell migration, proliferation, differentiation, and angiogenesis. In the present study, the primary promoter of cell proliferation bFGF was selected as a model growth factor to enhance the wound healing effects of electrospun membranes. Though the growth factor has been successfully applied for bone repair as well as wound healing [23], in normal physiological conditions, its bioactivity in free form similarly to other growth factors is rapidly lost due to degradation, requiring the use of adequate delivery systems like electrospun membranes in this study to optimize their bioactivity and increase efficiency. Additionally to lengthening their plasma half time, effective delivery of these factors just like for chemical drugs reduces the side effects, controls the bioavailability, and avoids unstable serum levels [24, 25]. Hence, the heparin-binding site of the bFGF was exploited to carry bFGF on scaffolds; However, the distribution of the growth factor was only limited to the surface of the scaffold, which further prevented the continual release of bFGF and

its long-term activity [26]. Direct loading of the growth factor within scaffolds is also a possibility and helps lengthen the release time. In this context, electrospinning is currently widely used. This technique allows for the fabrication of scaffolds made of continuous fibers with diameters ranging from 100 to 5 mm and a three-dimension (3D) framework with high aspect ratio, high porosity, and very small pore size, which make them effective for drug delivery [27, 28]. Herein, electrospun scaffolds were made from graphene oxide (GO) and collagen (Col).

Graphene oxide, a derivative of carbon nanomaterial, has ignited increasing interest in various fields from electronics to biotechnology [29]. Its structure comprises carbon atoms that are condensed into a 2D honeycomb lattice with multiple oxygen groups including carboxyl, hydroxyl, and epoxy groups, decorated on the basal planes and edges. This special structure is responsible for the large specific surface area, high Young's modulus, good thermal conductivity and numerous functionalization sites of the molecule [30], good properties that give potential to GO in applications such as drug/gene delivery, biosensing, cancer therapy, tissue engineering, and other biomedical fields [31–33]. Due to its numerous -COOH and -OH groups and unique lamellar structure, GO can enhance the mechanical properties and biological interactions when functionalizing collagen, by providing more binding sites for bioactive growth factors or specific drugs [34]. Hence, it was utilized in this study for fabricating a nanofibrous scaffold for tissue engineering.

Collagen is the main ECM protein in skin and is of great interest in regenerative medicine due to its remarkable biocompatibility, water holding capacity, and biodegradability [35–37]. It can regulate cellular phenotype and cell-ECM interactions as well as modify the physicochemical properties of a scaffold to improve wound healing rate and quality [38]. However, the mechanical properties of collagen scaffolds are poor and the scaffolds are easily degraded at room temperature [39], which affects their drug release performance [40]. Thus, for improved stability, polylactic acid (PLA) was added into the preparation. PLA is a condensation thermoplastic elastomer with demonstrated low cytotoxicity and good biodegradability [41]. Most importantly, the raw material of PLA can be fabricated into different sizes and shapes by various common fabrication techniques such as electrospinning, plastic extrusion, casting, injection molding, and spin coating, or even 3D printing [42, 43]. Hence, the material is quite an attractive platform for various emerging applications in drug delivery, gene therapy, and regenerative medicine [44].

Overall, the aim of the present study was to prepare Col-GO-bFGF electrospun wound dressing biomaterials by combining GO, bFGF, and common natural macromolecular Col. In the attempt of slowing scaffold degradation, core–shell Col-GO/PLA nanofibrous scaffolds were also fabricated

using co-axial electrospinning. The physicochemical properties, drug release performance, and in vitro biocompatibility of the nanofiber scaffolds were thereafter systematically evaluated, before verifying the skin regeneration effect of the samples in rat full thickness skin wounds.

2 Materials and methods

2.1 Chemicals and reagents

All chemicals used were pure and of analytical grade. Type I collagen was purchased from Kele Biotech (China), graphene oxide from Suzhou Tanfeng Tech (China), and basic fibroblast growth factor (bFGF) from Pepro Tech (USA). Dulbecco's modified Eagle's medium (DMEM) and minimal essential medium (MEM) were purchased from Hyclone (USA), while fetal bovine serum (FBS), penicillin–streptomycin (PS), and other cell culture reagents were obtained from Gibco (USA). Meanwhile, fluorescein diacetate/propidium iodide (FDA/PI) and Cell Counting Kit-8 (CCK-8), as well as hematoxylin–eosin and Masson's trichrome kits, were procured from Sigma-Aldrich.

2.2 Animals

Animals (Adult SD rats, male, aged 8–10 weeks; weight: 180–220 g) were purchased from the animal center of Huazhong University of Science and Technology (HUST). They were kept in individual cages (22 ± 2 °C, humidity of 60–70%) under light/darkness cycles of 12 h each and fed a normal diet ad libitum. Experimentation protocols were approved by the Animal Ethical Committee of HUST.

2.3 Fabrication of the Col-GO-bFGF nanofiber scaffolds

For the Col-GO-bFGF scaffolds, Col (0.24 g) and GO (0, 0.12, 0.48, and 1.92 mg) were dissolved in hexafluoroisopropanol (HFIP) to prepare a 6% Col/HFIP solution that was further made into Col-GO solution with 0.05%, 0.2%, and 0.8% GO (weight percentages) respectively. The Col-GO solutions were then electrospun at 25–27 kV using a 19G needle, with an extrusion speed of 1 mL/h; 17 cm distance separated the spinneret and the collector (aluminum mesh). Col only solution served as control. Considering the high volatility of liquid HFIP, there was no concern that this solvent would remain in the electrospun matrix following processing, eliminating the need for further purification steps [45]. Samples were then cooled at – 20 °C, and freeze-dried in a vacuum lyophilizer, yielding the Col and Col-GO nanofiber scaffolds. Thereafter, some samples were placed in bFGF/PBS solution to load the 1 μg/mL

bFGF into the Col and Col-GO nanofiber scaffolds. This was done in static conditions and at room temperature, for 24 h. Finally, the samples were cut into disks of 1 cm in diameter, placed in 12-well plates, and sterilized by exposing to ultraviolet light overnight to obtain collagen-only membranes (Col), bFGF-loaded collagen membranes (Col-bFGF), collagen-GO hybrid membranes (Col-GO), and bFGF-loaded collagen-GO membranes (Col-GO-bFGF).

### 2.4 Fabrication of core–shell nanofibers by co-axial electrospinning

To fabricate the core/shell nanofibers (Fig. 1) two needles were used, an inner needle for the core fibers, and an outer needle for the shell. Only the 0.2% GO was selected for Col-GO composite preparation, based on the mechanical properties and drug release ability demonstrated by the monolayer electrospinning scaffolds. First, the Col-0.2% GO solution was delivered to the outer co-axial needle with a syringe pump. Then, neat PLA solution (6% wt/v) was prepared by dissolving in acetone/dimethylformamide (DMF) (80/20, v/v) at 60 °C for at least 6 h, under constant stirring; this was transferred to the inner needle with another syringe pump. Flow rates in the capillaries were controlled by these two separate pumps. The fluid flow rates of the core and shell solutions were 0.5 and 1.0 mL/h, respectively. The specific parameters defining the electrospinning system remained as described above. All electrospinning processes were performed at 25 °C and 60% humidity.

2.5 Morphological characterization

Freeze-dried membrane scaffolds were coated with gold nanoparticles and evaluated by scanning electron microscopy (SEM, JSM-IT300, JEOL, Japan) at a high voltage of 20 kV to observe their microstructure. The core/shell structure of the nanofibers was then evidenced by transmission electron microscopy (TEM, JEM-2100, JEOL, Japan). TEM samples were prepared by placing copper grids between the spinneret and the collector (aluminum mesh) and then depositing a thin layer of co-axial electrospun nanofibers onto the copper grids.

Attenuated total reflection-Fourier transform infrared spectroscopy (ATR-FTIR) and Raman spectroscopy were performed in VERTEX 70 (Bruker, Germany), using LabRAM HR800 (HORIBA JobinYvon, France) for recording the surface characteristics of the scaffolds. Lyophilized samples were utilized. FTIR measurements were carried out at a resolution of 4 cm^{-1} in the frequency range of 4000–500 cm^{-1} and the Raman spectrum was recorded at a scanning range of 50–4000 cm^{-1} [46]. The excitation source was a diode laser with a wavelength of

Fig. 1 Schematic illustration of the fabrication procedure of the different scaffolds
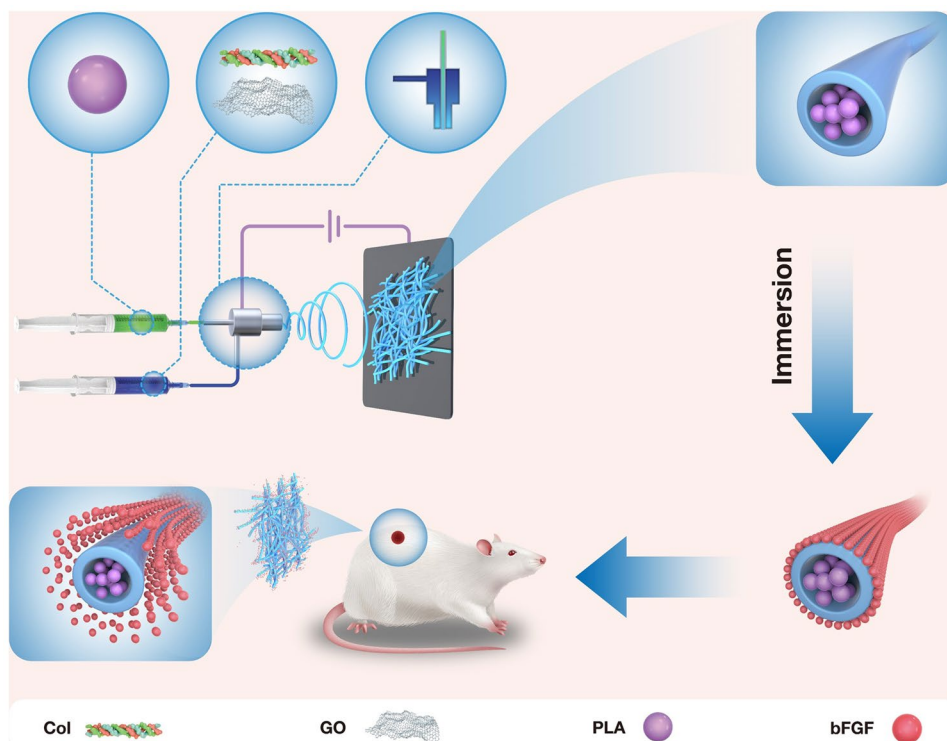
532 nm adjusted to a power of 30 mW. All data were then analyzed in OriginPro 2019 (OriginLab, America).

2.6 Mechanical testing of the scaffolds

An all-electric dynamic test instrument (ASTM D638, Instron) was used to measure the mechanical properties of the scaffolds. Tensile tests were performed according to the specifications of the instrument, with a load cell and extension speeds of 100 N and 5 mm/min, respectively. The OriginPro Software above was used to calculate the Young's moduli and plot the stress–strain curves.

2.7 Water contact angle measurements

To examine the hydrophilicity of the fabricated nanofibrous scaffolds, the dynamic water contact angle was measured by a contact angle analyzer (JGW-360B, China). The samples of each experimental group were cut into squares of 1 cm*1 cm and placed on the sample table to adjust the brightness of the light source before measurements. Then for each sample, 0.2 μL of pure water was dripped onto the surface of the latter, ensued with the analysis of the contact angle by the instrument's software. For each experimental group, three replicates were used.

2.8 Degradation rate measurements

The samples of each experimental group were cut into squares of 3 cm*3 cm, weighed and denoted as W0, and placed into 2 mL PBS(pH = 7.4) at 37 °C.

The membranes were removed at different time points (0, 1, 3, and 7 days), washed with distilled water 3 times, and then freeze-dried and weighed, denoted as Wi. For each experimental group, three replicates were used. The material weight loss is calculated by Eq. (1).

$$Material\ weight\ loss(\%) = (W0 - Wi)/Wo \times 100\% \tag{1}$$

2.9 In vitro cell experiments

2.9.1 NIH3T3 in vitro culture

NIH3T3 fibroblasts (ATCC, USA) were used to perform the cytological experiments. Briefly, the cells were cultured at 37 °C in DMEM containing 10% FBS and 1% PS, under an atmosphere with 95% air and 5% CO_2. Round electrospun membranes (diameter = 1 cm) were placed in 48-well plates to be sterilized under ultraviolet light (overnight). Then, cells at a concentration of 1×10^4 cells per/well were inoculated into each well and incubated with a complete medium. The medium was replaced every 3 days.

2.9.2 Cytocompatibility testing of the scaffolds

The scaffolds were cut into a 1-cm-diameter disks and placed into a 24-well plate to be sterilized under ultraviolet light (overnight). NIH3T3 cells were subsequently implanted onto different samples and cultured for 7 days to examine the cell compatibility of the scaffolds [47]. A live/dead assay was then performed, staining the cells with FDA/PI as directed by the manufacturer. Visualization was carried out under a confocal laser microscope (Leica Microsystems, Germany).

After 1, 4, and 7 days of culture, cell proliferation on the sample scaffolds was assessed using the CCK-8 assay. In brief, 100 μL of CCK-8 working solution was added to each well after replenishing the culture media; cultures were thereafter incubated at 37 °C for 1 h. Afterward, 100 μL supernatant aliquots were transferred to a new 96-well plate and their optical density (OD) values were determined using a microplate reader (BioTek ELx800, USA) at 450 nm.

2.9.3 Evaluation of cell migration

Human immortalized keratinocytes (HaCaT) were obtained from ProCell (CL-0090, Wuhan, China) and cultured in MEM medium supplemented with 15% FBS and 1% PS. HaCaT were seeded in 24-well plates at a density of 1×10^4 cells/well and cultured until they reached a 90% confluence. Next, cell migration under the influence of the scaffolds was evaluated. The fluid in each well was removed and replaced with a sample extract (scaffolds were immersed in 4 mL complete medium and placed in a 37 °C incubator for 24 h. In each test well, a scratch was made into the confluent cell layer using a pipette tip; cell migration was then monitored as the movement of the cells toward filling up the scratch, using an optical microscope (Olympus CKX41, Japan) which also served for capturing images at times 0, 8, 16, and 24 h of the experiment.

2.10 In vitro bFGF release

Scaffolds were immersed in 2 mL PBS solution and kept at 37 °C. At pre-determined time points (1, 3, 5, 7, 9, 11, 13, 15, 17, 19, 21, 23, 25, and 27 days), the supernatant was collected, and 2 mL fresh PBS was added in return. Then the collected bFGF supernatant was labeled, washed, chromogenic, and terminated by Elisa kit. Finally, the concentration of released bFGF in the supernatant was then determined spectrophotometrically using the method described in the growth factor instructions for use (Pepro Tech). Additionally, the loading capacity of the nanofiber scaffolds was calculated based on the maximum concentration of eluted bFGF in the collected PBS.

2.11 In vivo studies

All procedures were performed in accordance with the guidelines of the Animal Ethical Committee of HUST. Twelve adult SD rats were used. To minimize manipulation errors, all operations were performed by the same surgeon in a laminar clean bench under anesthesia (2% isoflurane inhalation). Shortly, on the dorsal sides of the animals, the hair was shaved, and the skin was disinfected, followed by the creation of circular full-thickness skin wounds of 1 cm in diameter. On each animal, four wounds were made, each for one of the four test samples (Blank, Col-GO/bFGF, PLA, and Co-axial/bFGF). Excisions were made by means of a wound model producer fabricated by molten 3D printing in the laboratory. Subsequently, wounded areas were treated with different scaffolds (individually), and gross images were recorded by cameras at different time points (0, 3, 7, and 14 days). Prior to scaffold implantation on the animals, sample sterilization was carried out according to the ISO 11137 standard requirements.

Histological analysis was performed after 14 days of treatment, following animal sacrifice by CO_2 asphyxiation. The wound together with the surrounding skin were excised and fixed in 10% formaldehyde. Tissues were then stained with hematoxylin–eosin (HE staining) and Masson's trichrome according to standard procedures to examine the epidermis, collagen deposition, and the formation of new tissue. On the rats, tissue samples were sectioned along the longest axis. Due to their irregular shape, three sections of each specimen were prepared for further histological analysis.

2.12 Statistical analyses

Statistical analysis was performed using GraphPad Software (USA). Data are shown as mean ± standard deviation. Parametric Student's t test and analysis of variance (ANOVA) with a post hoc test by Tukey's method were used to determine the significance levels. (*), (**), and (***) refer to the P values of < 0.05, < 0.01, and < 0.001, respectively.

3 Results and discussion

3.1 Morphology of the Col-GO scaffolds

Figure 2 shows the SEM images of the scaffolds viewed at lower and higher magnifications to enable the examination of sample morphology and the measurement of fiber diameters for different preparations. For the Col-GO scaffolds,
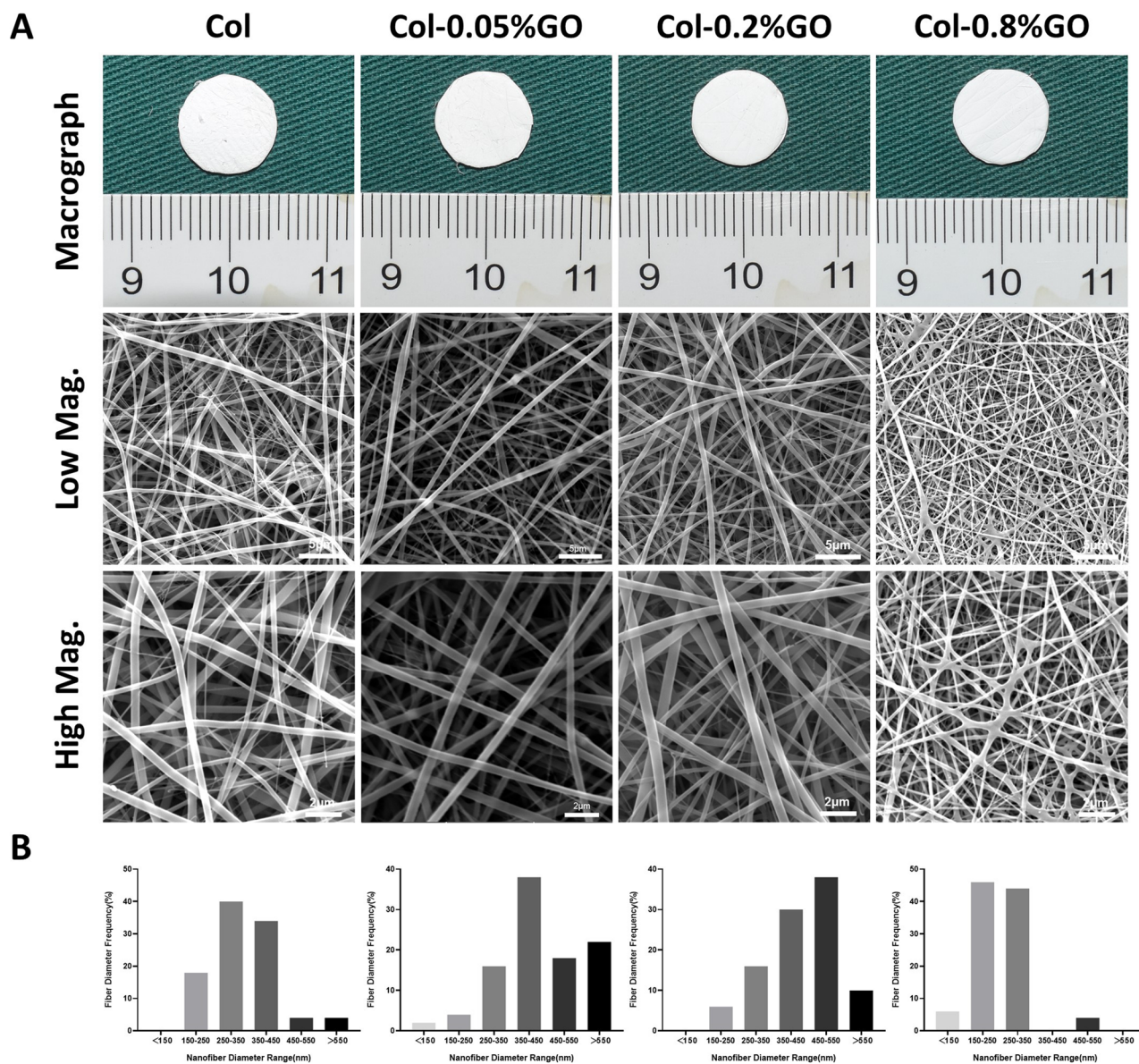
Fig. 2 Morphology of the Col-GO scaffolds. **A** FESEM images. **B** Distribution of nanofiber diameters within the Col-GO scaffolds

three (3) compositions were made, with different proportions of GO, namely 0.05, 0.2, and 0.8%, w/v. For each sample, the fiber size distribution is also represented. Overall, all electrospun samples appeared as randomly organized networks of nanofibers, the majority of which presented an average diameter between 150 and 550 nm. The meshed nanofibers thus formed 3D structures with high porosities and interconnected pores. Hence, at all tested GO concentrations, Col-GO scaffolds were successfully obtained by electrospinning. The Col-0.2% GO group stood out by its higher average fiber diameter which remained within 350 nm and 550 nm, propitious for cell attachment and growth (Fig. 3).

As shown in Fig. 4A, SEM was used to assess the morphology of fabricated core–shell scaffolds and to measure the fiber diameter of each sample. Morphologically, similar structures as for the samples obtained by simple electrospinning were obtained, with little disparities in fiber sizes. With the coaxial electrospinning, the diameter of the fibers ranged from 250 to 550 nm, while the nanofiber diameter of the scaffolds made of Col-GO and PLA alone was between 450 and 550 nm, and the nanofiber diameter of all groups of scaffolds was favorable for cell proliferation (Fig. 4A). The core–shell structure of the samples was further confirmed by TEM (Fig. 4B) which clearly indicated the bilayer structure of the samples produced by co-axial electrospinning.
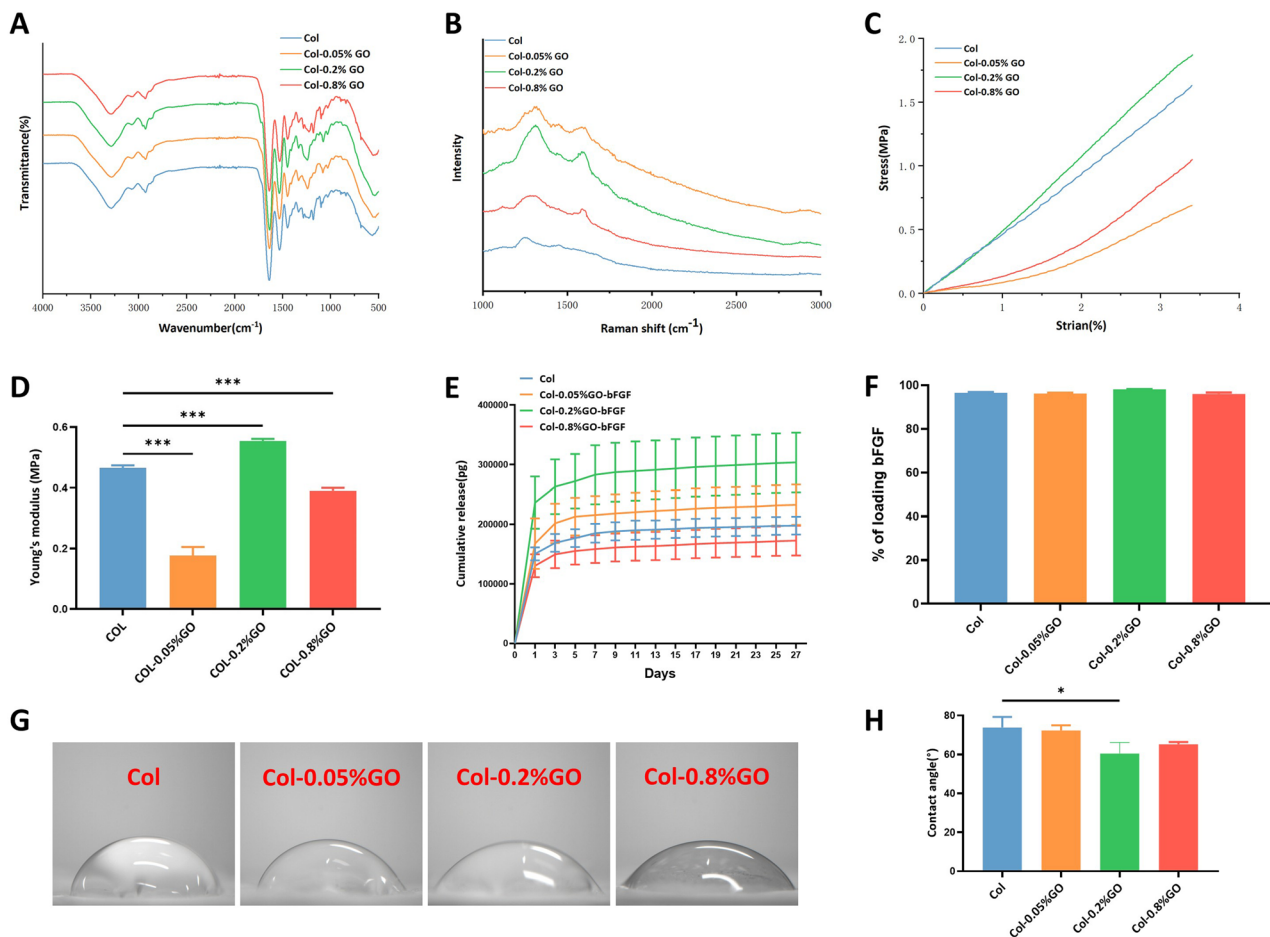
Fig. 3 Physico-chemical and mechanical properties of the Col-GO scaffolds. **A** ATR-FTIR spectra. **B** Raman spectra. **C** Stress–strain curves. **D** Young's moduli of the scaffolds. **E** Loading capacities of bFGF in the different groups. **F** Cumulative bFGF release profiles. **G** Water contact angles. **H** Water contact angle statistics chart

3.2 Physicochemical and mechanical properties of the Col-GO scaffolds

We then used the FTIR spectrum to confirm the chemical structures of the scaffolds and these results are shown in Fig. 3A. The results of Col and Col-GO membranes were consistent with literature reports [48]. In the FTIR spectrum, the -NH2 stretching vibration was detected as the peak at 3290 cm^{-1}, while the Fermi resonance overtone of the 1537 cm^{-1} band corresponded to 3081 cm^{-1}. The peak of C-H stretching was at 2933 cm^{-1}. Further, other peaks at 1641, 1537, and 1454 cm^{-1} were assigned to the C=O stretching, N–H bonding, and C-N stretching of amide (-CONH2) linkages in collagen. The C-N stretching of amine corresponded to the peak at 1233 cm^{-1}. To identify the GO in Col-GO scaffolds, we measured the Raman spectrum, a highly sensitive method for the detection of conjugated and double carbon–carbon bonds.

Raman spectroscopy provided helpful information on the structural characteristics of Col-GO nanofiber membranes. The spectra (Fig. 3B) displayed two evident peaks representing the G band (1590 cm^{-1}) and the D band (1309 cm^{-1}), which derived from in-plane vibrations of sp2 carbon atoms of the graphite lattice and the out-of-plane breathing mode of the sp2 atoms, respectively. These observations confirmed the layer separation of the GO structure, thus inferring the presence of GO in the composite samples.

The stress–strain curves of the different Col-GO scaffolds are shown in Fig. 3C. From these curves, the mechanical strength and Young's modulus (Fig. 3D) for each sample can be deduced using the highest point of the ordinate and the line slope of the linear part of the curves, respectively. The effect of GO on the mechanical properties of the composite samples varied with its concentration, with the optimum concentration to yield higher
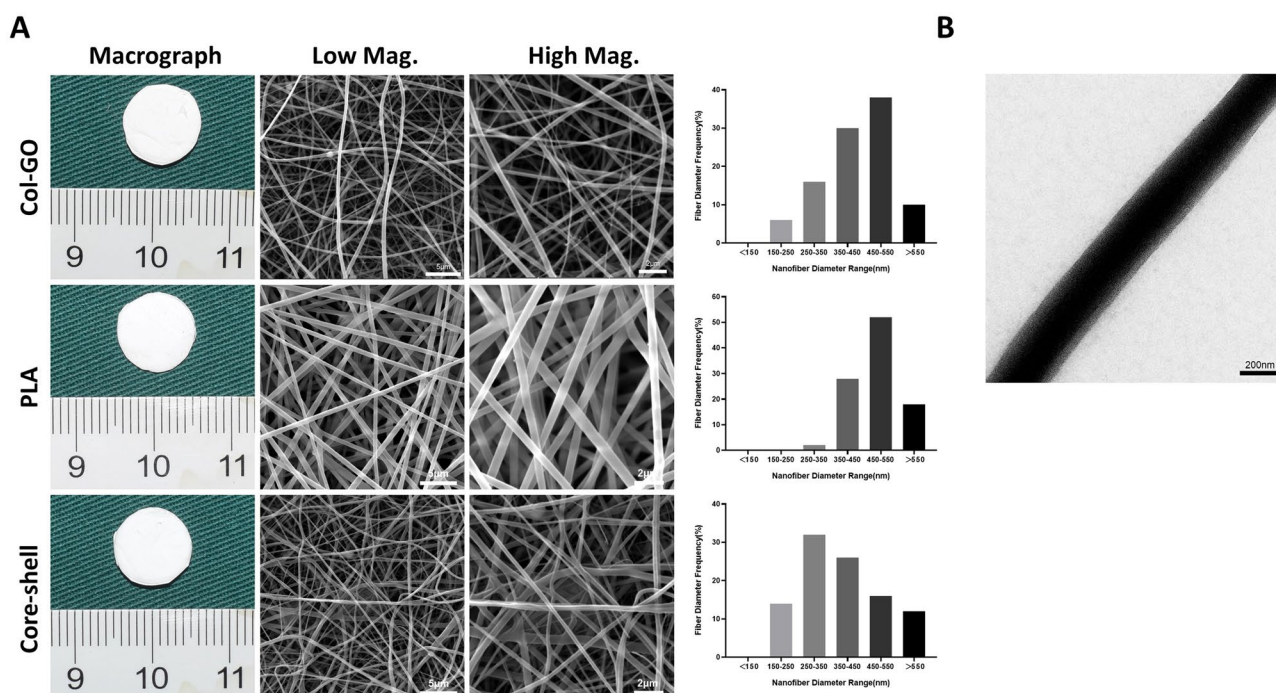
Fig. 4 Morphology of the co-axial electrospun scaffolds. **A** FESEM images and fiber diameter distribution. **B** TEM image of the Col-GO/PLA core–shell fibers

tensile strength and Young's modulus being 0.2%. At the lowest tested GO content however (Col-0.05% GO scaffold), the tensile strength and Young's modulus decreased relatively to the collagen-only sample, similarly to the observations made with the 0.8% GO sample (Col-0.05% GO). This suggests the existence of an equilibrium in the interaction between Col and GO and may be corroborated by the fiber size obtained with different preparations. In fact, the highest fiber diameter (Col-0.2% GO scaffolds) led to the top mechanical properties, while smaller fibers produced weaker samples. Besides, beyond a certain limit concentration, GO tends to aggregate, which also reduces the elasticity of the composite sample.

The water contact angle results of the nanofiber films are shown in Fig. 3G–H. Overall, all sample types displayed an average water contact angle less than 90°, indicating their hydrophilic nature. In the scaffolds, the obtained values were lower than that observed for the pure Col sample ($73.85 \pm 5.434°$) though not significantly except for Col-0.2% GO, the hydrophilic properties of scaffolds were effectively altered by the addition of moderate concentrations of GO. Col-0.2% GO exhibited the smallest water contact angle value ($60.48 \pm 5.673°$), suggesting its highest hydrophilicity and emphasizing its greatest potential for supporting cellular activities.

3.3 In vitro drug release

The drug release profiles of bFGF from different samples are presented in Fig. 3E, and their loading capacities in Fig. 3F. There was no significant difference in the loading capacity among scaffolds, probably because the presence of graphene oxide had no direct effect on the loading capacity of the drug. However, the Col-0.2% GO-bFGF group had the highest cumulative release of bFGF of $30.94 \pm 7.77\%$. Because the concentration of graphene oxide directly affects the drug release, too high or too low a concentration of graphene oxide is not conducive to the drug release. Regardless, there was sustained drug release from day 1 to day 27 in all scaffold types.

3.4 Physicochemical and mechanical properties of the co-axial electrospun scaffolds

Based on the previous material characteristics and drug sustained release results, we finally selected the single-layer electrospinning Col-0.2% GO group with better results as the shell layer of coaxial electrospinning, and we also selected PLA as the core layer of coaxial electrospinning. The physicochemical properties of coaxial scaffolds were compared with PLA scaffolds and monolayer electrostatic spinning scaffolds.
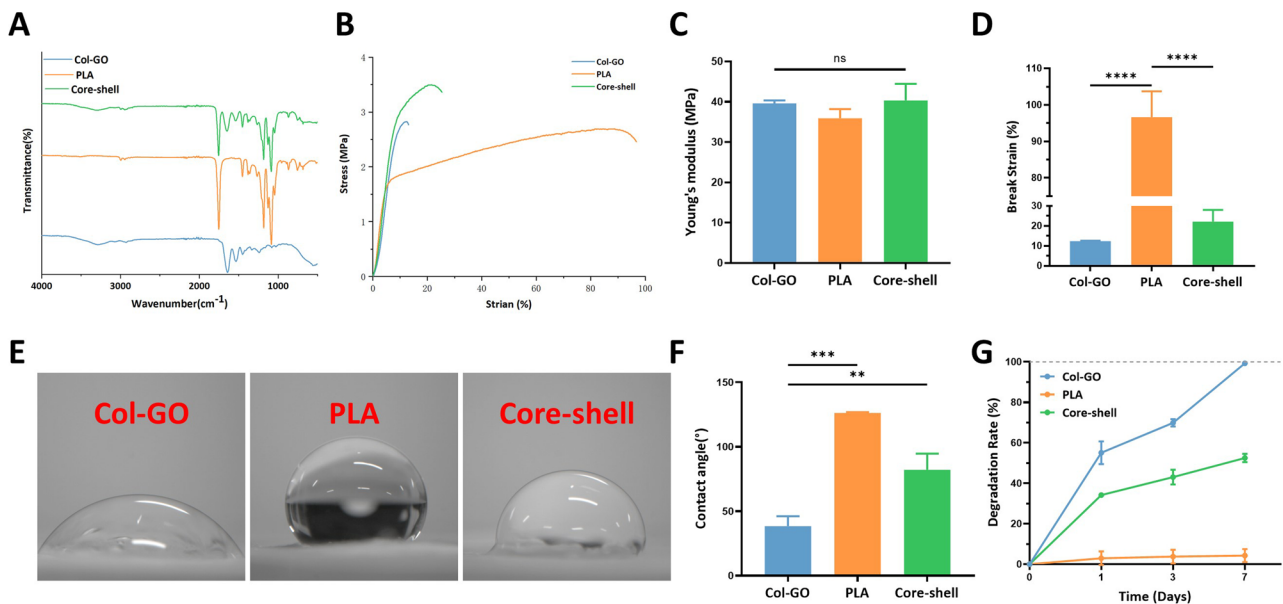
Fig. 5 Physico-chemical and mechanical properties of the core–shell scaffolds. **A** ATR-FTIR spectra. **B** Raman spectra. **C** Young's moduli of the scaffolds. **D** Strain at fracture break. **E** Water contact angles. **F** Water contact angle statistics chart. **G** Degradation of rate

The infrared spectra of the samples are shown in Fig. 5A. In the spectra, the C-H stretch peaks at 2941 cm^{-1}, while the peaks at 1641 cm^{-1}, 1537 cm^{-1}, and 1454 cm^{-1} are attributed to the C=O stretch, N–H bond, and C-N stretch for amide (-CONH2) linkages in collagen, respectively. In addition, the characteristic peaks of PLA at 1749 cm^{-1} (C=O stretching) and 1453 cm^{-1} (-CH3 bending) were also evident. Hence, the core–shell composite scaffold associated the peaks of both Col-GO and PLA, confirming the successful co-axial electrospinning process.

The mechanical properties of the composite core–shell samples are presented in Fig. 5B–D. The Young's modulus of the co-axial electrospun scaffolds was comparable to that of the Col-GO materials fabricated by simple electrospinning as well as to the PLA control sample. However, the strain at break was higher for the PLA scaffolds, and decreased for the core–shell samples, while Col-GO presented the poorest strain. Hence, incorporating PLA in the samples enhanced their elasticity.

The water contact angles of the samples are presented in Fig. 5E, F. The Col-GO group exhibited the smallest water contact angle (60.48 ± 5.673°), indicating the highest hydrophilicity. Then the core–shell scaffold (82.18 ± 12.48°) showed moderate hydrophilicity. Finally, the PLA sample (126.2 ± 0.706°) showed the worst hydrophilicity. The degradation results of this study (Fig. 5G) showed that all scaffolds began to degrade after 1 day. After 7 days, the Col-GO scaffold was almost completely degraded, with a degradation rate of 99.33 ± 0.577%. The PLA group had almost no degradation, with a degradation rate of 4.28 ± 3.188%, while the core–shell scaffold had a moderate degradation rate of 52.52 ± 2.046%, indicating that the scaffold would not be easily degraded. It is beneficial to the application of stents in wound healing. Indeed, through its hydrophobicity, PLA reduces the hydrophilicity of the composite bilayer samples, which would improve their stability in the aqueous environment and minimize degradability.

3.5 In vitro biocompatibility of the scaffolds

Live-dead assay was performed on NIH3T3 cells to assess the cytotoxicity of the produced samples; results are presented in Fig. 6A. After 7 days culture, no dead cells could be detected on the different samples; the cell density was the highest in the Col-GO/bFGF followed by core–shell scaffolds (loaded with bFGF), while the PLA samples generated the lowest cell density. These suggested the improved cell survival and proliferation rates on the first two (2) scaffolds when considered with the latter. These results were consistent with the CCK-8 test results at day 7 (Fig. 6B). In conclusion, the generated Col-GO/bFGF and core–shell/bFGF scaffolds have good biocompatibility in vitro.

Results of the scratch test assay with HaCaT cells are shown in Fig. 6C. The core–shell/bFGF and the Col-GO/bFGF groups showed better cell migration-promoting abilities, with the lowest scratch sizes at the end of the 24 h experiment (Fig. 6D). Interestingly, the fastest keratinocytes migration rate of 43.59 ± 1.35% was derived from the core–shell/bFGF scaffolds.
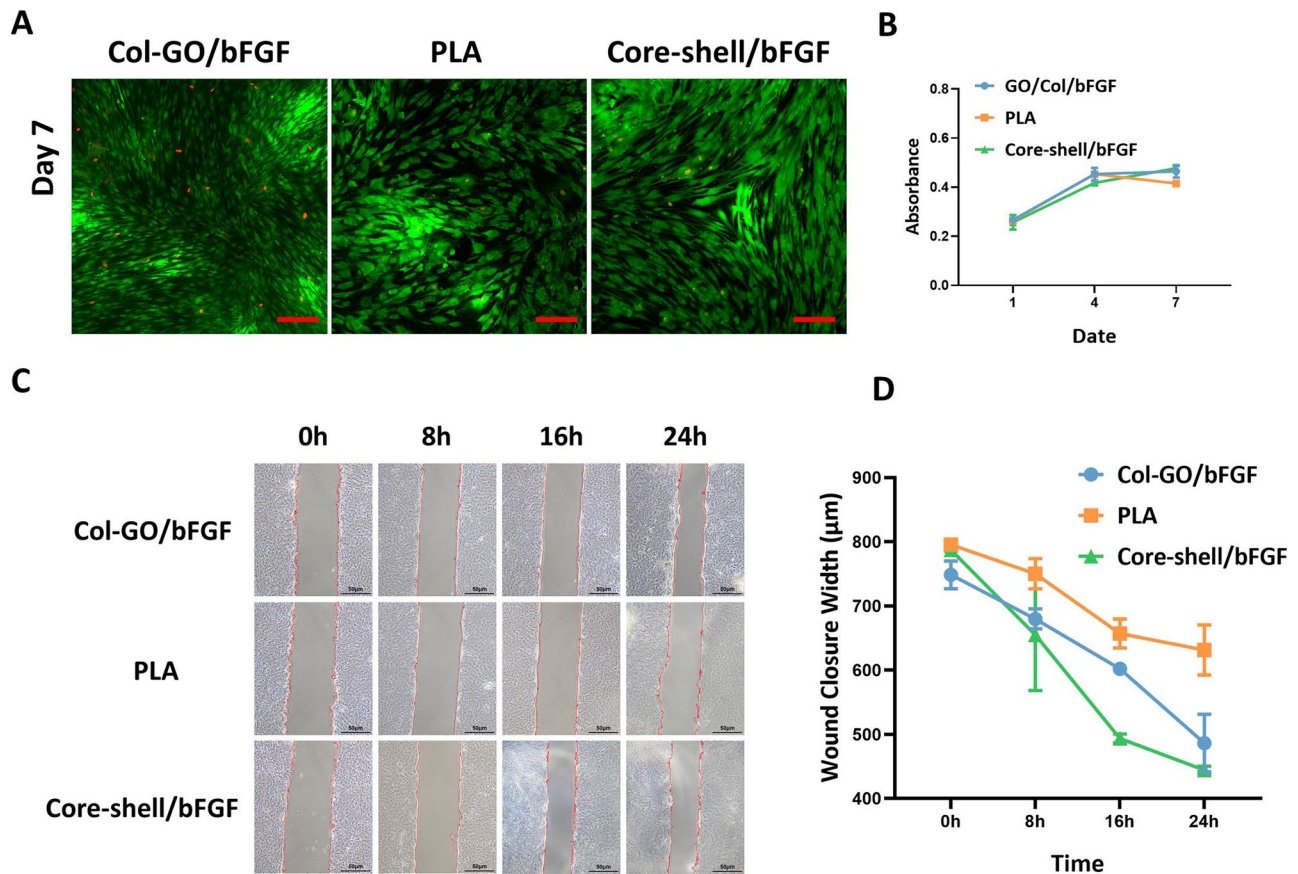
Fig. 6 In vitro biocompatibility of the scaffolds. **A** Confocal fluorescent images showing results of FDA/PI staining of NIH3T3 cells cultured on the scaffolds for 7 days (scale bars: 100 μm). **B** Results of CCK-8 assay performed on NIH3T3 cells seeded on the scaffolds. **C** Images of the scratch test of keratinocytes showing cell migration

3.6 Effects of the scaffolds on in vivo wound healing

The healing of full thickness skin defects was assessed in adult rats over 14 days using the herein developed scaffolds as dressings (Fig. 7). The Col-GO/bFGF (with 0.2% GO), PLA, and core–shell/bFGF membranes were applied and compared with wounds without any treatment used as blank control at four (4) different time points (0, 3, 7, and 14 days). In the first 3 days, the col-Go /bFGF and core–shell /bFGF groups showed better-wound healing rates, $34.90 \pm 8.38\%$ and $35.73 \pm 2.23\%$, respectively, which shows that the scaffolds loaded with bFGF can better promote wound healing in the early stage. Similarly, on day 7, the Col-GO/bFGF and core–shell/bFGF groups of scaffolds had better-wound healing rates of $47.95 \pm 1.49\%$ and $42.22 \pm 2.44\%$, respectively. On day 14 however, a very significant difference was observed when comparing the aforementioned group with the others, with the healing rate in the PLA-covered wound being the lowest. Moreover, the Col-GO/bFGF membrane was well pasted on the wound and then implanted subcutaneously.

This treatment group showed complete wound healing at day 14, with $96.39 \pm 0.66\%$ wound closure, while the healing rates were at $92.29 \pm 0.42\%$, $81.23 \pm 2.55\%$, and $72.33 \pm 3.71\%$ in the core–shell/bFGF, blank and PLA groups, respectively.

Histological investigations were further carried out using the HE and Masson's trichrome stainings (Fig. 8). Unhealed areas were distinguished from normal or fully healed areas by subcutaneous tissue examination. The sections with incomplete tissue healing show little coloration indicative of absence for skin structures like hair follicles, sebaceous glands, and other skin attachments, and this extends over relatively long tissue portions. The unhealed area which reflects the state of the wound healing process was also analyzed, using the images of the HE staining. In the Col-GO/bFGF-treated samples, however, the length of the wound that remained amounted to 999.731 ± 183.796 μm, which was comparable to that in the core–shell/bFGF group (882.506 ± 84.657 μm) while those for other groups were much higher (3737.522 ± 78.730 μm for the blank, 2589.454 ± 133.709 μm for PLA).
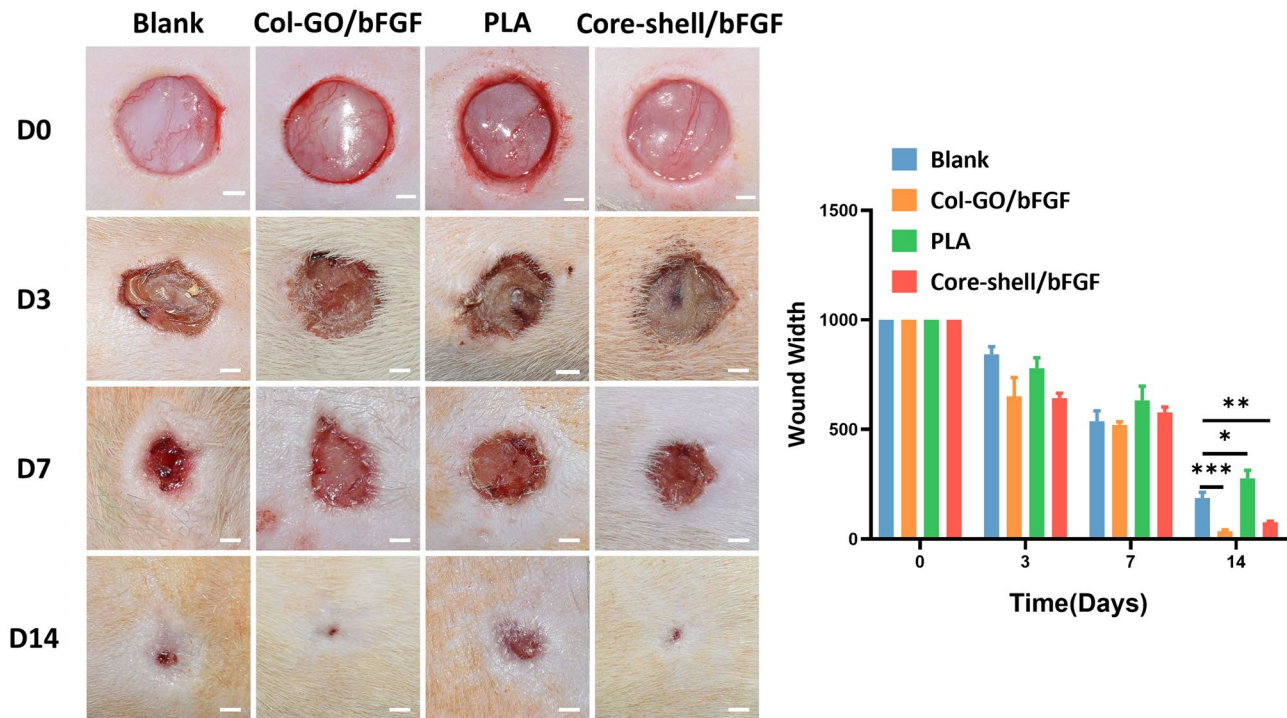
Fig. 7 In vivo test results. **A** Macro views of four groups treated with the scaffolds (scale bar 200 μm). **B** Percentage of unhealed wound area at different time points after treatment

The thickness of the new epidermis which reflects the state of the wound healing process was also analyzed, using the images of the Masson's trichrome staining. It was of 155.593 ± 36.665 μm for the Col-GO/bFGF group, and 105.789 ± 9.923 μm for the core–shell/bFGF group, but thinner for the others (blank: 94.008 ± 9.816 μm; PLA: 57.649 ± 17.095 μm) confirming the retarded healing process therein. The Masson staining further indicated the irregular arrangement of the new collagen in these two last groups (blank and PLA) with a high degree of inflammatory cell infiltration, supporting the above conclusions. In the other two groups however, the collagen bundles were highly deposited, with uniform and regular arrangement. This indicated that the Col-Go/bFGF and core–shell/bFGF group have better wound healing effects than the blank and PLA groups.

Skin defects caused by burn, trauma, tumor resection, and various other conditions are still a major problem in clinical practice; therefore, promoting wound healing with high quality has always been a hot spot and difficulty in clinical research. Compared with traditional autologous skin transplantation, tissue-engineered skin has the advantages of extensive sources and no donor site injury and is a promising treatment for achieving high-quality wound healing [49].

Skin ECM is composed of collagen, fibronectin, laminin, glycosaminoglycan, and proteoglycan as well as a variety of adhesive proteins that form a network of fibers with a diameter of 260–410 nm and a length of tens of microns [37, 38]. From the perspective of material bionics, nanofibers produced by electrospinning technology can highly simulate the 3D topological structure of such ECM [39]. Collagen represents a natural ECM that can be applied to wound healing, but its physical and mechanical properties are poor, as it is easy to tear and easy to degrade [40]. Therefore, applying collagen directly to the wound has some disadvantages, such as poor therapeutic effect. As a new flexible material with excellent performance, GO can be used as a scaffold to cross-link with other biomaterials, which can improve the mechanical and biological properties of the composite scaffold. Therefore, the mixture with GO is expected to make up for the above deficiencies of collagen. We prepared Col-GO nanofiber film by electrospinning technology. This scaffold is expected to have good drug release performance, good mechanical properties and good biocompatibility, and provide a good structural microenvironment for wound healing. To further meet the biological microenvironment of wound healing, bFGF was integrated to the electrospun film. On the other hand, the aim was to improve the efficiency of bFGF application, while functionalizing the Col-GO film scaffold. Thus, making up for mutual deficiencies of different components of the new composite was the target, to effectively promote wound healing.
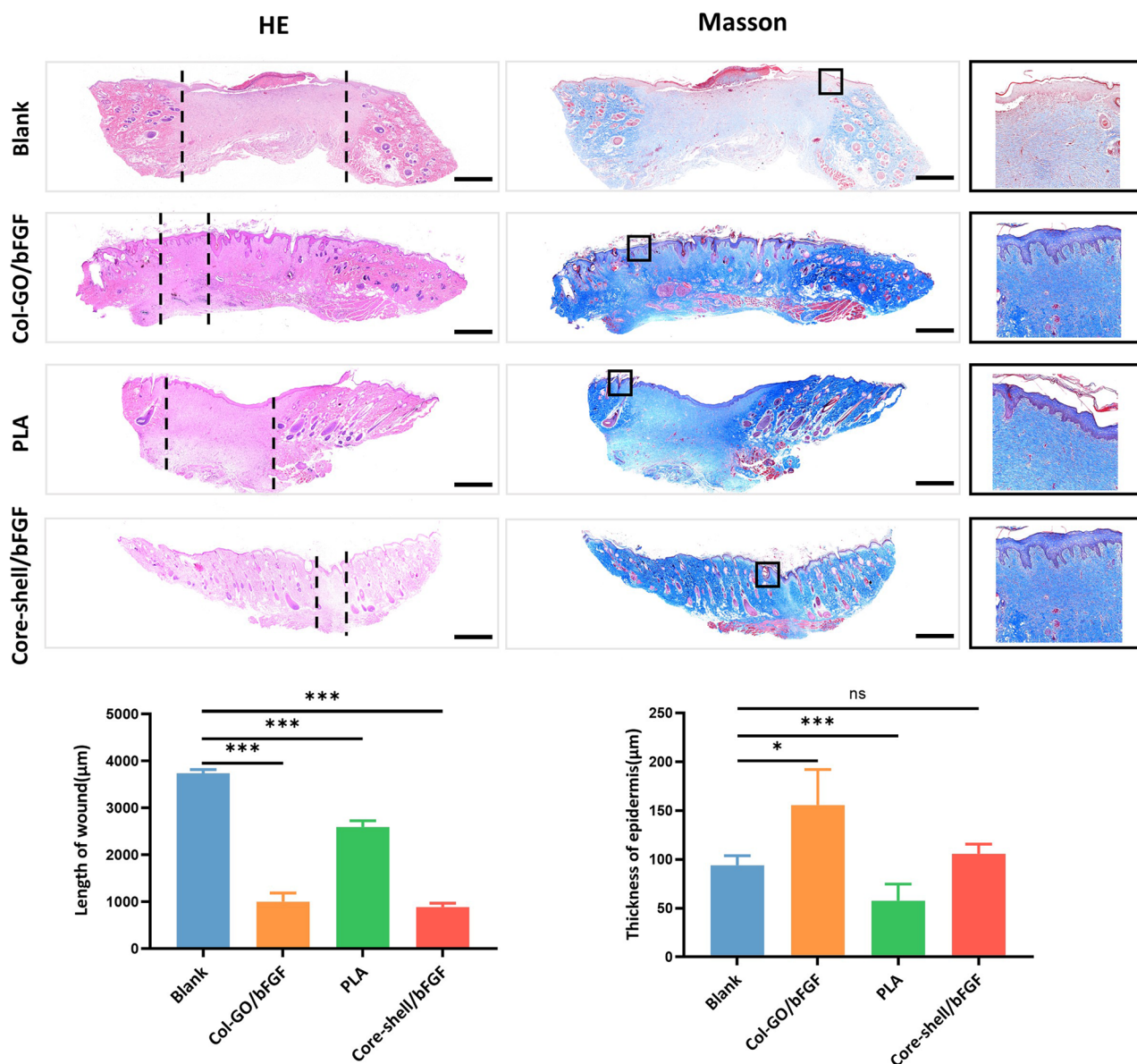
Fig. 8 HE staining and Masson staining of wound Sects. 14 days after treatment. Section between the black dashed lines: unhealed area, scale bar 1000 μm. The magnified area shows the thickness of the epidermal layer as indicated by the black square box; scale bar 400 μm

Based on the studies of Li and Zeng et al. [50] and on our previous research results [51], we selected 6% (w/v) Col and GO with different concentrations to prepare the electrospun samples. Morphological analysis was done by SEM. Compared with Col, Col 0.05% GO, and Col 0.8% GO scaffolds, the surface of the Col-0.2% GO group showed more porous microstructure, with more uniform distribution of nanofibers. Moreover, the fiber diameter in this composite was suitable for cell growth, indicating better suitability for wound healing. Due to the wound healing application, the hydrophilicity of the materials is an important parameter as this reflects permeability and conductivity to cell proliferation and migration, with high hydrophobicity limiting the contact of the material with the wound and impairing nutrient supply. The water contact angle measurements which portray material hydrophilicity showed that the water contact angle of the electrospun nanofibers was less than 90° in each group. Thus, all groups displayed good hydrophilicity.

The mechanical properties test results show that the elastic modulus of Col-0.2% GO scaffold is the highest. Adding GO can significantly optimize the mechanical properties of Col electrospun film, but the strengthening of mechanical properties is not directly proportional to the concentration of GO. Adding too high a concentration of collagen to GO may

cause the material to become more brittle. Only by adding a moderate concentration of GO can improve the mechanical properties of the material. From our experiment, it is found that 0.2% GO can effectively increase the mechanical properties of Col-GO electrospun film.

To further functionalize the Col-GO nanofiber electrospun membrane, bFGF was loaded into the Col-GO nanofiber electrospun scaffold. The sustained release results showed that both Col-0.2% GO-bFGF and Col-bFGF electrospun scaffolds had a consistent and stable sustained release ability. In addition, the Col-0.2% GO-bFGF electrospun scaffold released more growth factors than the Col-bFGF electrospun scaffold. However, there was no significant difference in the drug loading rate between the two groups, a result that was attributed to the excellent drug-carrying properties of the collagen in the scaffold.

To further enhance the mechanical properties of Col-GO/bFGF electrospun nanofiber membranes, slow down their degradation, and better utilize the slow-release efficacy of bFGF, we used co-axial electrospinning to process the polymeric materials, with PLA as the core layer and Col-GO as the shell layer; a core–shell structured nanofiber membrane was generated. The membrane was shown to be moderately hydrophilic and could better slow down the degradation of the material in in vitro experiments. In cytological experiments, the live/dead assay showed that the electrospun scaffolds of Col-GO/bFGF and core–shell/bFGF groups had better biocompatibility, and the density of NIH3T3 cells grown on these scaffolds was significantly higher than that in the PLA group, showing good ability to promote cell proliferation. Meanwhile, the CCK8 assay also showed that the numbers of cells in the Col-GO/bFGF and core–shell/bFGF groups were more than that in the PLA group, showing their best ability to promote cell proliferation, as in the live/dead cell staining. The results of scratch experiments showed that the healing areas for Col-GO/bFGF and core–shell/bFGF groups were the best at 24 h. Overall, the constructed Col-GO/bFGF and core–shell/bFGF nanofiber scaffolds have good biocompatibility, good ability to promote cell proliferation and migration, and have good drug release properties. Compared with Col-GO stents, core–shell stents have moderate hydrophilic properties and material degradability, which are more conducive to wound healing.

In the in vivo experiments, we observed that Col-GO/bFGF and core–shell/bFGF electrospun scaffolds had a significant promotion effect on the healing of skin defects in rats.

In conclusion, the combination of 0.2% GO and collagen better improved the mechanical properties of the electrospun scaffold, promoted cell proliferation and migration, and enhanced the efficiency of drug release. The loading of bFGF and its subsequent constant release promoted skin wound healing, which is a promising exogenous source of wound healing

for clinical application. It should be noted that although the core–shell scaffolds loaded with growth factors we prepared achieved the purpose of promoting wound healing, they did not achieve perfect scar-free wound healing, so it is necessary to develop tri-axial, nanofibers with 3D structure, etc. through further research to better simulate the microenvironment of wound healing and control the activation level of fibroblasts to prevent fibrosis, collagen metabolism disorder, and scar formation, to achieve scar-free wound healing [52].

4 Conclusion

We have demonstrated that bFGF loaded into GO-functionalized collagen nanofiber membranes promoted rapid repair of a circular incision of 1 cm in diameter in the full thickness of rat skin. This was due to its strong mechanical properties and controlled release of bFGF. These properties promoted cell proliferation and migration in vitro. The scaffolds also enhanced wound repair in vivo indicating a promising application in wound healing. Meanwhile, coaxial electrospun scaffolds containing PLA material can slow down the degradation of the material and have moderate hydrophilic properties compared with monolayer electrospun scaffolds, which have wider application prospects than monolayer electrospun wire scaffolds.

Author contributions All authors contributed to the study conception and design. Material preparation, data collection, and analysis were performed by [Jialong Chen], [Guo Zhang], [Yang Zhao], [Muran Zhou], [Aimei Zhong], and [Jiaming Sun]. The first draft of the manuscript was written by [Jialong Chen] and all authors commented on previous versions of the manuscript. All authors read and approved the final manuscript.

Declarations

Conflict of interest The authors declare no conflict of interest.

References

1. Chen L, Xing Q, Zhai Q et al (2017) Pre-vascularization enhances therapeutic effects of human mesenchymal stem cell sheets in full thickness skin wound repair. Theranostics 7(1):117–131. https://doi.org/10.7150/thno.17031

2. Martin P (1997) Wound healing--aiming for perfect skin regeneration. Science 276(5309): 75–81. https://doi.org/10.1126/science.276.5309.75

3. Lo ZJ, Lim X, Eng D et al (2020) Clinical and economic burden of wound care in the tropics: a 5-year institutional population health review. Int Wound J 17(3): 790–803. https://doi.org/10.1111/iwj.13333

4. Sen CK (2021) Human wound and its burden: updated 2020 compendium of estimates. Adv Wound Care (New Rochelle) 10(5): 281–292. https://doi.org/10.1089/wound.2021.0026

5. Guest JF, Ayoub N, McIlwraith T et al (2017) Health economic burden that different wound types impose on the UK's National Health Service. Int Wound J 14(2):322–330. https://doi.org/10.1111/iwj.12603

6. Guo S, Dipietro LA (2010) Factors affecting wound healing. J Dent Res 89(3): 219–229. https://doi.org/10.1177/0022034509359125

7. Pallaske F, Pallaske A, Herklotz K et al (2018) The significance of collagen dressings in wound management: a review. J Wound Care 27(10):692–702. https://doi.org/10.12968/jowc.2018.27.10.692

8. Tao SC, Guo SC, Li M et al (2017) Chitosan wound dressings incorporating exosomes derived from MicroRNA-126-overexpressing synovium mesenchymal stem cells provide sustained release of exosomes and heal full-thickness skin defects in a diabetic rat model. Stem Cells Transl Med 6(3):736–747. https://doi.org/10.5966/sctm.2016-0275

9. Chouhan D, Mandal BB (2020) Silk biomaterials in wound healing and skin regeneration therapeutics: From bench to bedside. Acta Biomater 103:24–51. https://doi.org/10.1016/j.actbio.2019.11.050

10. Zheng L, Li S, Luo J et al (2020) Latest advances on bacterial cellulose-based antibacterial materials as wound dressings. Front Bioeng Biotechnol 8:593768. https://doi.org/10.3389/fbioe.2020.593768

11. Choi S, Zo S, Park G et al (2020) Preparation of Waterborne Polyurethane-Based Macroporous Sponges as Wound Dressings. J Nanosci Nanotechnol 20(8):4634–4637. https://doi.org/10.1166/jnn.2020.17827

12. Wang X, Ding B, Li B (2013) Biomimetic electrospun nanofibrous structures for tissue engineering. Mater Today (Kidlington) 16(6): 229–241. https://doi.org/10.1016/j.mattod.2013.06.005

13. Wang C, Chu C, Zhao X et al (2021) The diameter factor of aligned membranes facilitates wound healing by promoting epithelialization in an immune way. Bioactive Materials 11:206–217. https://doi.org/10.1016/j.bioactmat.2021.09.022

14. Urbanczyk M, Layland SL, Schenke-Layland K (2020) The role of extracellular matrix in biomechanics and its impact on bioengineering of cells and 3D tissues. Matrix Biology 85–86:1–14. https://doi.org/10.1016/j.matbio.2019.11.005

15. Boni BOO, Lamboni L, Bakadia BM et al (2020) Combining silk Sericin and surface micropatterns in bacterial cellulose dressings to control fibrosis and enhance wound healing. Engineered Science 10:68–77. https://doi.org/10.30919/es8d906

16. Dong Y, Kong J, Phua SL et al (2014) Tailoring surface hydrophilicity of porous electrospun nanofibers to enhance capillary and push-pull effects for moisture wicking. ACS Appl Mater Interfaces 6(16):14087–14095. https://doi.org/10.1021/am503417w

17. Zhang L, Wang Z, Xiao Y et al (2018) Electrospun PEGylated PLGA nanofibers for drug encapsulation and release. Mater Sci Eng C Mater Biol Appl 91:255–262. https://doi.org/10.1016/j.msec.2018.05.045

18. Ziyadi H, Baghali M, Bagherianfar M et al (2021) An investigation of factors affecting the electrospinning of poly (vinyl alcohol)/kefiran composite nanofibers. Adv Compos Hybrid Mater 1–12. https://doi.org/10.1007/s42114-021-00230-3

19. Liu Y, Chen X, Liu Y et al (2022) Electrospun coaxial fibers to optimize the release of poorly water-soluble drug. polymers (Basel) 14(3):469. https://doi.org/10.3390/polym14030469

20. Zhou H, Shi Z, Wan X et al (2019) The relationships between process parameters and polymeric nanofibers fabricated using a modified coaxial electrospinning. Nanomaterials (Basel) 9(6):843. https://doi.org/10.3390/nano9060843

21. Zhang M, Song W, Tang Y et al (2022) Polymer-Based Nanofiber-Nanoparticle Hybrids and Their Medical Applications. Polymers (Basel) 14(2):351. https://doi.org/10.3390/polym14020351

22. Ning T, Zhou Y, Xu H et al (2021) Orodispersible membranes from a modified coaxial electrospinning for fast dissolution of diclofenac sodium. Membranes (Basel) 11(11):802. https://doi.org/10.3390/membranes11110802

23. Cai S, Liu Y, Zheng Shu X et al (2005) Injectable glycosaminoglycan hydrogels for controlled release of human basic fibroblast growth factor. Biomaterials 26(30): 6054–6067. https://doi.org/10.1016/j.biomaterials.2005.03.012

24. Julier Z, Park AJ, Briquez PS et al (2017) Promoting tissue regeneration by modulating the immune system. Acta Biomater 53:13–28. https://doi.org/10.1016/j.actbio.2017.01.056

25. Chen L, Liu J, Guan M et al (2020) Growth factor and its polymer scaffold-based delivery system for cartilage tissue engineering. Int J Nanomedicine 15:6097–6111. https://doi.org/10.2147/ijn.S249829

26. Nilasaroya A, Kop AM, Morrison DA (2021) Heparin-functionalized hydrogels as growth factor-signaling substrates. J Biomed Mater Res A 109(3): 374–384. https://doi.org/10.1002/jbm.a.37030

27. Bhattarai RS, Bachu RD, Boddu SHS et al (2018) Biomedical applications of electrospun nanofibers: drug and nanoparticle delivery. Pharmaceutics 11(1):5 https://doi.org/10.3390/pharmaceutics11010005

28. Xu S, Deng L, Zhang J et al (2016) Composites of electrospun fibers and hydrogels: a potential solution to current challenges in biological and biomedical field. J Biomed Mater Res B Appl Biomater 104(3): 640–656. https://doi.org/10.1002/jbm.b.33420

29. Shin SR, Li YC, Jang HL et al (2016) Graphene-based materials for tissue engineering. Adv Drug Deliv Rev 105(Pt B): 255–274. https://doi.org/10.1016/j.addr.2016.03.007

30. Song HS, Kwon OS, Kim JH et al (2017) 3D hydrogel scaffold doped with 2D graphene materials for biosensors and bioelectronics. Biosens Bioelectron 89(Pt 1): 187–200. https://doi.org/10.1016/j.bios.2016.03.045

31. Mei Q, Liu B, Han G et al (2019) Graphene oxide: from tunable structures to diverse luminescence behaviors. Adv Sci (Weinh) 6(14): 1900855. https://doi.org/10.1002/advs.201900855

32. Shamekhi MA, Mirzadeh H, Mahdavi H et al (2019) Graphene oxide containing chitosan scaffolds for cartilage tissue engineering. Int J Biol Macromol 127:396–405. https://doi.org/10.1016/j.ijbiomac.2019.01.020

33. Zhou M, Lozano N, Wychowaniec JK et al (2019) Graphene oxide: a growth factor delivery carrier to enhance chondrogenic differentiation of human mesenchymal stem cells in 3D hydrogels. Acta Biomater 96:271–280. https://doi.org/10.1016/j.actbio.2019.07.027

34. Bharadwaz A, Jayasuriya AC (2020) Recent trends in the application of widely used natural and synthetic polymer nanocomposites in bone tissue regeneration. Mater Sci Eng C Mater Biol Appl 110:110698. https://doi.org/10.1016/j.msec.2020.110698

35. Das P, DiVito MD, Wertheim JA et al (2020) Collagen-I and fibronectin modified three-dimensional electrospun PLGA scaffolds for long-term in vitro maintenance of functional hepatocytes. Mater Sci Eng C Mater Biol Appl 111:110723. https://doi.org/10.1016/j.msec.2020.110723

36. Homaeigohar S, Boccaccini AR (2020) Antibacterial biohybrid nanofibers for wound dressings. Acta Biomater 107:25–49. https://doi.org/10.1016/j.actbio.2020.02.022

37. Ucar B, Humpel C (2018) Collagen for brain repair: therapeutic perspectives. Neural Regen Res 13(4): 595–598. https://doi.org/10.4103/1673-5374.230273

38. Levingstone TJ, Ramesh A, Brady RT et al (2016) Cell-free multi-layered collagen-based scaffolds demonstrate layer specific regeneration of functional osteochondral tissue in caprine joints. Biomaterials 87:69–81. https://doi.org/10.1016/j.biomaterials.2016.02.006

39. Semenycheva LL, Egorikhina MN, Chasova VO et al (2020) Enzymatic hydrolysis of marine collagen and fibrinogen proteins in the presence of thrombin. Mar Drugs 18(4):208 https://doi.org/10.3390/md18040208

40. Rong ZJ, Yang LJ, Cai BT et al (2016) Porous nano-hydroxyapatite/collagen scaffold containing drug-loaded ADM-PLGA microspheres for bone cancer treatment. J Mater Sci Mater Med 27(5):89. https://doi.org/10.1007/s10856-016-5699-0

41. Li G, Zhao M, Xu F et al (2020) Synthesis and biological application of polylactic acid. Molecules 25(21):5023. https://doi.org/10.3390/molecules25215023

42. Tyler B, Gullotti D, Mangraviti A et al (2016) Polylactic acid (PLA) controlled delivery carriers for biomedical applications. Adv Drug Deliv Rev 107:163–175. https://doi.org/10.1016/j.addr.2016.06.018

43. Kim M, Jeong JH, Lee JY et al (2019) Electrically conducting and mechanically strong graphene-polylactic acid composites for 3D printing. ACS Appl Mater Interfaces 11(12): 11841–11848. https://doi.org/10.1021/acsami.9b03241

44. Barata D, Dias P, Wieringa P et al (2017) Cell-instructive high-resolution micropatterned polylactic acid surfaces. Biofabrication 9(3): 035004. https://doi.org/10.1088/1758-5090/aa7d24

45. Bürck J, Heissler S, Geckle U et al (2013) Resemblance of electrospun collagen nanofibers to their native structure. Langmuir 29(5): 1562–1572. https://doi.org/10.1021/la3033258

46. Vukosavljevic B, Murgia X, Schwarzkopf K et al (2017) Tracing molecular and structural changes upon mucolysis with N-acetyl cysteine in human airway mucus. Int J Pharm 533(2): 373–376.https://doi.org/10.1016/j.ijpharm.2017.07.022

47. Wang S, Wang Z, Foo SE et al (2015) Culturing fibroblasts in 3D human hair keratin hydrogels. ACS Appl Mater Interfaces 7(9): 5187–5198. https://doi.org/10.1021/acsami.5b00854

48. Selvaraj S, Fathima NN (2017) Fenugreek incorporated silk fibroin nanofibers—a potential antioxidant scaffold for enhanced wound healing. ACS Appl Mater Interfaces 9(7): 5916–5926. https://doi.org/10.1021/acsami.6b16306

49. Bhardwaj N, Chouhan D, Mandal BB (2017) Tissue engineered skin and wound healing: current strategies and future directions. Curr Pharm Des 23(24): 3455–3482. https://doi.org/10.2174/1381612823666170526094606

50. Li J, Zhou C, Luo C et al (2019) N-acetyl cysteine-loaded graphene oxide-collagen hybrid membrane for scarless wound healing. Theranostics 9(20): 5839–5853. https://doi.org/10.7150/thno.34480

51. Zeng Y, Zhou M, Chen L et al (2020) Alendronate loaded graphene oxide functionalized collagen sponge for the dual effects of osteogenesis and anti-osteoclastogenesis in osteoporotic rats. Bioact Mater 5(4): 859–870. https://doi.org/10.1016/j.bioactmat.2020.06.010

52. Finnerty CC, Jeschke MG, Branski LK et al (2016) Hypertrophic scarring: the greatest unmet challenge after burn injury. Lancet 388(10052): 1427–1436. https://doi.org/10.1016/s0140-6736(16)31406-4

Publisher's Note Springer Nature remains neutral with regard to jurisdictional claims in published maps and institutional affiliations.